PCCP

Accepted Manuscript

ROYAL SOCIETY OF CHEMISTRY

www.rsc.org/pccp

Collisionally-Induced Dissociation Products of the Protonated Dipeptide Carnosine: Structural elucidation, Fragmentation Pathways and Potential energy surface analysis.

Eslam M. Moustafa,[a] Ida Ritacco,[b] Emilia Sicilia,[b] Nino Russo[b][c] and Tamer Shoeib[a][d]*

[a]Department of Chemistry, The American University in Cairo, New Cairo 11835, Egypt.

[b]Dipartimento di Chimica Universita della Calabria, Via P. Bucci, cubo 14c, 87036 ArcaVacata di Rende (CS), Centro di Calcolo ad Alte Prestazioni per Elaborazioni Parallele e Distribuite - Centro d'Eccellenza MIUR, Rende 87036, Italy.

[c]Division de Ciencias Basicas e Ingenieria, Departamento de Quimica, Universidad, Autonoma Metropolitana-Iztapalapa, Av. San Rafael Atlixco No. 186, Col. Vicentina, CP 09340, Mexico, Distrito Federal Mexico

[d]Centre for Analytical Science, Department of Chemistry, Loughborough University, Loughborough, Leicestershire LE11 3TU, UK.

* T.Shoeib@aucegypt.edu

Abstract

Collision-induced dissociation (CID) experiments on protonated carnosine , $[Carnosine + H]^+$ using several collision energies were shown to yield eleven different fragment ions with the product ions $[Carnosine - H_2O + H]^+$ and $[Carnosine - NH_3 + H]^+$ to be the lowest energy processes. Energy-resolved CID showed that at slightly higher collision energies the ions $[Histidine + H]^+$ and $[Histidine - H_2O - CO + H]^+$ are formed. At even higher energies four other product ions were observed, however, attained relatively lower abundances. Quantum chemistry calculations, carried out at different levels of theory, were employed to probe fragmentation mechanisms that account for all the experimental data. All the adopted computational protocols give similar energetic trends and the range of the calculated free energy barrier values for the generation of all the observed product ions is in agreement with the fragmentation mechanisms offered here.

Introduction

The dipeptide β-alanine-L-histidine, also known as carnosine, is a naturally occurring substance synthesized by endogenous carnosine synthetase discovered more than 100 years ago [1]. It is present at elevated levels in human skeletal and cardiac muscles as well as in brain tissue [2-5] and is typically concentrated in the cytosol of cells due to its water solubility [6]. Although not much is known about its physiological function, several possible roles have been considered since its first discovery [7, 8] such as pH-buffering [9], metal chelation [10] or neurotransmitter function [11]. Carnosine is also reported to have antioxidant activity due to its ability to react with several highly reactive species, such as hydroxyl, super oxide and molecular oxygen free radicals, especially in the water rich environment inside the body [3, 12, 13]. More recently, carnosine was shown to play a role in the detoxification of the anti-cancer drug oxaliplatin, one of the most commonly used Pt-anticancer chemotherapeutic agents [14]. Additionally, it was shown that complexes formed between carnosine and oxaliplatin reduce the efficacy of the Pt-drug causing increased viability in cancer cells [14].

The interaction of carnosine with metals of biological relevance was the subject of several studies including the reporting on metal binding energies to the peptide and providing structural elucidation of the complexes and the resulting collision induced dissociation (CID) products [14-21]. Studies of the CID products of protonated carnosine on the other hand have received considerably less attention. In general, the observed fragmentation patterns generated from protonated peptides ions typically depend on several factors including the amino acid composition, the size of the peptides, the excitation method used and the charge of the ions [22]. CID of protonated peptides employing soft ionization techniques such as electrospray and matrix assisted laser desorption proved useful for determining amino acid sequences. This in turn increased the interest in the fragmentation pathways of protonated

peptides and the mechanisms of product ion formation which spurred several studies on protonated α-amino acids [23-30] while studies on β-amino acids or peptides that contain those remain very sparse [31, 32].

Relatively simple CID mass spectra are generated due to the fragmentation of protonated aliphatic α-amino acids which mainly show their respective iminium ions produced via the concomitant loss of H_2O and CO. Hydroxylic and acidic α-amino acids lose H_2O through the OH and COOH groups in their side chains in addition to the concomitant loss of H_2O and CO. Basic α-amino acids such as arginine and lysine have the a nitrogen on the side chain as the favoured site of protonation [30] thus one of the major fragmentation pathways in these amino acids involve the loss of NH_3 and, in the case of protonated arginine, guanidine [23,24]. Facile elimination of NH_3 is observed in all aromatic α-amino acids, with the exception of protonated histidine in addition to the concomitant elimination of H_2O and CO [23, 33-36]. At higher collision energies, subsequent to the elimination of NH_3 the losses of H_2O, CO, CO_2 and CH_2CO are observed while losses of HCN, $HCNH_2$, and NH_3 take place subsequent to the concomitant losses of H_2O and CO [26].

Protonated peptide fragmentation under low-energy collision conditions are believed to be charge induced and electron rearrangements involved in decomposition of an activated ion into two or more fragments are assumed to be triggered by localization of charge on specific sites within the molecular structure of the decomposing ions [22]. Thus, the observation of a large number of product ions typically implies that there is a heterogeneous population of fragmenting precursor isomers. This situation is likely since peptides contain multiple functional groups and each of them can act as a protonation site. In the case of carnosine these sites include the carboxylic, amino, and amide groups as well as the imidazole moiety of histidine. The average pK values of these groups are 2.64 for the carboxylic, 6.77 for the *tele* nitrogen of imidazole and 9.37 for the amino group [10]. This large range of values may

explain the fact that carnosine can exist in several different tautomeric forms. In addition to possibly having a large population of fragmenting precursor isomers it is also possible, however, for inter-conversions between these protonated isomers to occur if low energy barriers are required, which can also contribute to the formation of a large number of collisionally-induced fragment ions.

In this paper, we report for the first time on a detailed examination of the CID products of protonated carnosine and employ quantum chemistry calculations to rationalize the observed fragmentation patterns.

Instrumentation

An LTQ linear ion trap mass spectrometer (Thermo Electron, San Jose, CA, USA) and an Acquity TQ tandem quadrupole mass spectrometer, (Waters, MA, USA) both equipped with electrospray ionisation interfaces were used in this work. Carnosine, HPLC-grade water and methanol were all purchased from Sigma-Aldrich, UK. Deuterium exchange experiments were carried out in solutions that contain deuterium oxide (99.9 %) and CH_3OD (99.5 % both from Sigma-Aldrich). The LTQ Resolving powers achieved were in the order of 1500 while the upper instrumental error limit in measurements was 0.2 m/z units. The LTQ auto-tune routine was used to obtain lens, quadrupole and octapole voltages for maximum transmission of the ions of interest. Helium gas, admitted into the ion trap at a maintained pressure of approximately 10^{-3} Torr, was used as the buffer gas to improve the trapping efficiency and as the collision gas for collision-induced dissociation experiments performed here. Experiments designed to elucidate ion structures or fragmentation pathways on the LTQ were performed as follows: the ion of interest was selected then collisionally activated by setting the activation amplitude at 25–35% of the maximum voltage available (determined empirically),

and the activation Q setting (used to adjust the frequency of the RF excitation voltage) was set at 0.25 units.

The Acquity TQ was operated in positive ion mode, with typical values of cone and extractor voltages set to 30, and 3 respectively. The capillary voltage was optimised day to day for maximum signal transmission and spray stability, the optimised range was typically 2200-2500 volts. The de-solvation gas was usually set at a flow of 250 L h^{-1} and a temperature of 150 °C. Argon was used as the collision gas at a typical flow rate of 0.15 ml min^{-1}. Ions sampled from the electrospray suffered many collisions in an attempt to achieve effective thermalization in the lens region, being from the orifice/skimmer to the first r.f. only quadrupole. The bias potential in this lens region was set up to strike a compromise between signal transmission and minimal collisional heating. The precursor ions underwent multiple collisions with argon to produce tandem mass spectra obtained at collision energies in the range 0-30 eV in the lab frame having both Q1 and Q3 operated at unit resolution with typical a dwell time of 25 millisecond per transition. Both instruments described here were previously successfully employed by us using the exact set up described to elucidate structures of metal and non-metal containing biological ligands. [37-39] While some of our previous studies were conducted near single collision conditions [40-42] the experiments reported here were all performed under multiple collision conditions.

Computational Methods

All molecular orbital calculations were performed using GAUSSIAN 09 [43]. Structures were fully optimized without symmetry constraints by means of density functional theory (DFT) using the hybrid Becke's three-parameter exchange functional and the correlation functional from Lee, Yang and Parr (B3LYP) [44-46] in conjunction with the standard Pople basis set 6-311++G(d,p) [47-49]. All critical points obtained here were characterised by

harmonic frequency calculations as either minima or first order saddle point. All the stationary points reported here were further characterized by harmonic frequency analysis to have the appropriate number of imaginary frequencies, which are none for local minima and one for first-order saddle points. Intrinsic reaction coordinate calculations [50] were run to connect the transition state geometries with those of the corresponding minima. All species considered in this work were in the singlet state and thus all calculations performed were on closed shell species. The spin has been conserved through all the reactions described within the manuscript. Total energies, zero-point energies, thermal corrections and entropies are given in Supplementary Tables S1-S4. Long and weak interactions such as hydrogen bonds are often difficult to accurately describe by DFT theory. However, studies employing DFT calculations with the B3LYP functional accurately detail hydrogen bonding in small systems such as hydrogen fluoride dimers, clusters of cyanoacetylene and hydrogen cyanide as well as in water dimers and complexes [51-54]. The B3LYP and the 6-31++G(d,p) combination was successfully used to model internal hydrogen bonding within a protonated triglycine and to demonstrate the validity of the "mobile proton" model in the tripeptide [55] while the B3LYP/6-311++G(2d,2p) level of theory was shown to predict the existence of a hydrogen bonding stabilised zwitterionic form of protonated carnosine in the gas phase [21]. With the aim of comparison, however, both single point MP2 (frozen core) [56] and M06 [57] calculations by using the same 6-311++G(d,p) basis set on optimized B3LYP/6-311++G(d,p) geometries were carried out. The hybrid M06 exchange-correlation functional was employed here as it is specifically designed to accurately describe non-covalent interactions. Additionally, the M06 functional along with the 6-311++G(d,p) basis set was employed to perform full optimization followed by frequency calculations of geometrical structures of minima and transition states and to map the fragmentation pathways on the corresponding PESs. For the sake of clarity, from this point forward the used levels of theory B3LYP/6-

311++G(d,p), M06/6-311++G(d,p), M06/6-311++G(d,p)//B3LYP/6-311++G(d,p) and MP2/6-311++G(d,p)//B3LYP/6-311++G(d,p) will be indicated as B3LYP, M06, M06SP, MP2SP, respectively.

Results and discussion

Electrospraying a 1 mM solution of carnosine in a 1:1 (v/v) water-methanol solution generated the mass spectra shown and assigned in Figure 1 (see panel A). The MS^2 spectra of $[carnosine + H]^+$, for which the potential energy surfaces were extensively studied and found to be relatively flat containing several low energy structures, [21] is shown in Figure 1 (see panel B). Collision-induced dissociation experiments are shown to yield eleven different fragment ions as shown in Figure 1 (see panel B) and Figure 2. It is important to note that results shown on Figures 1 and 2 were produced by two different mass spectrometers operated by two different collision gases and not under single collision conditions. Thus even at the same values of E_{lab} no direct comparison of ion intensities between the two figures is possible. Although many pathways leading to the formation of such fragments were examined, only those at lower energies are reported here. Relative gas-phase free energies of minima and transition states are calculated with respect to the most stable conformer of $[carnosine + H]^+$, **227** shown in Figures 3 and 4, which has also been previously reported as the lowest energy species for protonated carnosine [17, 21, 58] obtained by protonation at the *pros* imidazole nitrogen of the imidazole ring of the histidine residue and containing two pseudo rings. The first is a pseudo eight membered ring due to the formation of a hydrogen bond between the hydrogen atom of the protonated *pros* imidazole nitrogen and the amide carbonyl oxygen atom. The second of such pseudo rings is formed through the formation of a hydrogen bond between the hydrogen atom of the amide nitrogen and the nitrogen atom of the amino group. The outcomes of all the employed levels of theory, that is B3LYP, M06, M06SP and MP2SP are reported and discussed.

Many of the fragment ions observed in the MS^2 spectra shown in Figure 1 (see panel B) were previously reported [17, 18]. The MS^2 spectra of [carnosine-d_5 + D]$^+$ in which carnosine has all its labile hydrogen atoms exchanged with deuterium atoms is shown in Figure S1 of the supplementary material.

[Carnosine – CH_2NH + H]$^+$

The ion at m/z 198 shown in Panel B of Figure 1, which is assigned as [carnosine – CH_2NH + H]$^+$ is shown to be formed from the most stable conformer of [carnosine + H]$^+$, **227**, through the transition state $\mathbf{TS_{227\rightarrow198}}$ with an associated barrier of 49.7, 52.3, 64.0 and 62.0 kcal mol^{-1} calculated at the B3LYP, M06, M06SP and MP2SP levels respectively as shown in Figure 3. Schematic representations and optimised structures at the B3LYP level of all involved species are shown in Figure 4 and Figure S2 in the supplementary material respectively. This ion is shown to correspond to the signals at m/z 203 and 204 at a ratio of 4:1 in the CID spectrum of the deuterium-incorporated complex shown in Figure S1. This indicates that the loss of a single deuterium atom most likely on the nitrogen atom of the eliminated CH_2ND to be the dominate pathway but that evidence of gas phase H/D exchange prior to the elimination reaction observed.

[Carnosine - CH_2NH - H_2O + H]$^+$

The subsequent elimination of H_2O from the ion [carnosine – CH_2NH + H]$^+$ to produce [carnosine - CH_2NH - H_2O + H]$^+$, which is observed at m/z 180 in Figure 1 corresponds to a signal cluster at m/z 183, 184, 185 and 186 in the in the CID spectrum of the deuterium-incorporated complex shown in Figure S1. This cluster indicates the loss of up to three deuterium atoms most likely due to the elimination of CH_2ND and D_2O as consistent with the proposed fragmentation pathway. The presence of such a signal cluster is also an indication

of significant H/D gas phase scrambling prior to the elimination reaction observed. This partial H/D gas phase scrambling has been previously reported in the CID of protonated and metal ion bound-aromatic amino acids including histidine and tryptophan [25, 26, 42]. Mechanisms rationalising this observed H/D scrambling were reported [42] in which it is assumed that the forward and reverse rate of each of the steps are fast, an assumption that is reasonable as hydride transfers typically have fast reaction rates [25]. The proposed fragmentation pathway to produce [carnosine - CH_2NH - H_2O + H]$^+$ is shown in Figure 3 to go through a transition state calculated to be at 51.0, 56.2, 65.7 and 55.4 kcal mol^{-1} at the B3LYP, M06, M06SP and MP2SP levels relative to structure **227**, respectively. It is important to note that for three of the used computational protocols, the second transition state shown in Figure 3 is calculated to be very slightly higher in energy than the first transition state shown on the figure. This energy difference where $\mathbf{TS_{198\rightarrow180}}$ is shown to be higher than $\mathbf{TS_{227\rightarrow198}}$ is calculated to be at a maximum of 3.9 kcal mol^{-1} at the M06SP level while at the MP2SP level the order is shown to be reversed with $\mathbf{TS_{198\rightarrow180}}$ being lower by 6.6 kcal mol^{-1}. This may consequently explain, the relatively low abundance observed for the ion [carnosine - CH_2NH + H]$^+$.

[Carnosine – NH_3 +H]$^+$

The CID curve shown in Figure 2 reveals that the loss of NH_3 pathway to produce the ion at m/z 210 from the precursor [carnosine + H]$^+$ at m/z 227 as shown in Figure 1 is among the lowest energy processes. The CID spectrum of the deuterium-incorporated complex shown in Figure S1 indicates the losses of ND_3, NHD_2 and NH_2D to be evident at approximate ratios of 5:4:1. This significant H/D scrambling prior to the elimination of NH_3 was previously reported in metal ion containing and protonated amino acids. [26, 42] The calculated energy profile for this reaction is shown in Figure 5, and the corresponding schematic representations

and optimised structures at the B3LYP level of all involved species are shown in Figure 6 and Figure S3 in the supplementary material respectively. The loss of NH_3 from [carnosine + H]$^+$ to form [carnosine – NH_3 +H]$^+$ observed at m/z 210 in Figure 1 is shown to go through the transition state $\mathbf{TS_{227\rightarrow 210}}$ in which the hydrogen bond of structure **227** between the hydrogen atom of the amide nitrogen and the nitrogen atom of the neutral amino group is no longer present and a 1,3-hydride shift to the terminal amino nitrogen takes place. This transition state $\mathbf{TS_{227\rightarrow 210}}$ leads to the release of NH_3 and the formation of an ion molecule adduct as shown in structure **210** in Figures 6 and S3, in which the remaining ion forms a hydrogen bond with the newly liberated NH_3 molecule through the hydrogen of the amide atom. This rather long and weak hydrogen bonding interaction, being at 1.977 and 1.937 Å as optimized at the B3LYP and M06 levels respectively is then very easily broken to produce the ion observed at m/z 210. The production of this ion is shown to be among the lowest processes calculated here, requiring an activation barrier of 47.1 kcal mol^{-1}, at the B3LYP level, calculated with respect to the lowest energy form of protonated carnosine, as shown in Figure 5. This same energy barrier is calculated to be the 44.8, 57.5 and 53.7 kcal mol^{-1} at the M06, M06SP and MP2SP levels respectively.

All efforts to locate a 'loose' transition state for the direct removal of NH_3 from Structure **227** in Figures 6 and S3 resulted into a concerted transition state for the simultaneous shifting of two hydrogen atoms: the first from the amide nitrogen to the terminal amino nitrogen, forming the NH_3 which is subsequently lost as a neutral fragment, while the second being one of the two hydrogen atoms on the CH_2 adjacent to the CO shifting to the amide nitrogen atom. This step was calculated at the B3LYP level of theory to have a barrier of 72.1 kcal mol^{-1} relative to structure **227** of Figures 6 and S3. The second step in this pathway is the removal of NH_3 involving a subsequent transition state which was calculated to have a barrier of 37.3 kcal mol^{-1} relative to structure **227** of Figures 6 and S3. This process detailed here is

shown in supplementary Figure S5 and is calculated to be less viable than the one previously described in Figures 5 and 6 for the loss of NH_3.

[Carnosine - NH_3 - H_2O + H]$^+$

The subsequent loss of H_2O from the ion [carnosine – NH_3 +H]$^+$ observed at m/z 210 in Figure 1 is shown in Figure 5 to occur by overcoming the transition state **$TS_{210\rightarrow192}$** schematically shown in Figures 6 and S3, in which the backbone of the dipeptide is rearranged to allow for the carbonyl oxygen atom of the -COOH group to abstract the hydrogen atom of the *pros* nitrogen of the imidazole ring which in turn allows for the elimination of H_2O and formation of a bond between the carbon atom of the remaining carbonyl group and the *pros* nitrogen of the imidazole ring resulting in the formation of a five-member ring within the ion [Carnosine - NH_3 - H_2O + H]$^+$ which is observed at m/z 192. The corresponding signal cluster for this ion in the CID spectrum of the deuterium-incorporated complex shown in Figure S1 indicates the losses of one, two, three, four or five deuterium atoms at ratios of 1:6:10:3:2 which is consistent with the mechanism proposed here. The transition state **$TS_{210\rightarrow192}$** for this process is calculated to be only very slightly higher in energy than the transition state **$TS_{227\rightarrow210}$** responsible for the generation of the ion [Carnosine - NH_3 + H]$^+$ at m/z 210.

[Carnosine - NH_3 - H_2O - CO + H]$^+$

The subsequent loss of CO from the ion [Carnosine - NH_3 - H_2O + H]$^+$ produces the ion [Carnosine - NH_3 - H_2O - CO + H]$^+$ observed at m/z 164 in Figure 1. This process in which the CO in the five-member ring of the ion [Carnosine - NH_3 - H_2O + H]$^+$ is eliminated, as it is shown in Figures 5 and 6, to produce the structure **164** going through the transition state

$TS_{192\rightarrow164}$ calculated to be at 50.3 kcal mol^{-1} at B3LYP level relative to structure **227**, this value increases to 61.0, 70.0 and 59.5 at the M06, M06SP and MP2 levels respectively.

$[Carnosine - H_2O + H]^+$ and $[Carnosine - H_2O - CO + H]^+$

The ion at m/z 209 shown in panel B of Figure 1 is shown in Figure 7 to be produced initially at relatively low collision energies; however, it does not attain any significant relative abundance. This ion was assigned to be due to the loss of H_2O from the precursor $[Carnosine + H]^+$ at m/z 227 shown in Figure 1, the corresponding signal for this ion in the CID spectrum of the deuterium-incorporated complex shown in Figure S1 is observed at m/z 213 and 214 indicating the losses D_2O and HOD respectively. This ion is proposed to be formed by overcoming the barrier relative to the transition state **$TS_{227\rightarrow209}$** shown in Figure 7 in which a very similar rearrangement to the transition state **$TS_{210\rightarrow192}$** where H_2O is eliminated from $[Carnosine - NH_3 + H]^+$. Here, however, the resulting ion $[Carnosine - H_2O + H]^+$ is observed at m/z 209 as shown in Figure 1 and the barrier for the corresponding transition state was calculated to be 43.0, 42.0, 52.0 and 43.2 kcal mol^{-1} at B3LYP, M06, M06SP and MP2 levels, respectively which is in line with our experimental observation of the formation of the ion at m/z 209 being a relatively low energy process.

The subsequent neutral loss of CH_2NH from the resulting ion $[Carnosine - H_2O + H]^+$ at m/z 209 is shown to proceed via a C-C bond cleavage and a hydride transfer of one of the hydrogens on the terminal amino nitrogen atom to a carbonyl oxygen atom on the peptide to produce the observed ion $[Carnosine - H_2O - CH_2NH + H]^+$ at m/z 180 and the neutral fragment CH_2NH as shown in Figures 6 and S3. While this process may be consistent with the signal cluster around m/z 184 in the CID spectrum of the deuterium-incorporated complex shown in Figure S1, this pathway proceeds through the transition state **$TS_{209\rightarrow180B}$** shown in Figure 7 which is calculated to be 63.6, 70.5, 72.6 and 73.3 kcal mol^{-1} as calculated

at the B3LYP, M06, M06SP and MP2 levels, respectively with respect to structure **227** to produce structure **180B** shown in Figures 6, S3 and 7. This is compared to the favoured production route of structure **180** via the pathway shown in Figure 3 which proceeds through the transition state $\mathbf{TS_{198\rightarrow180}}$ calculated at 51.0, 56.2, 65.7 and 55.4 kcal mol^{-1} for the same levels of theory respectively.

The loss of CO from the ion [Carnosine - H_2O + H]$^+$ at m/z 209 produces the ion [Carnosine - H_2O - CO + H]$^+$ which is observed at m/z 181 in Figure 1 and corresponding signals at m/z 185 and 186 in the CID spectrum of the deuterium-incorporated complex shown in Figure S1 consistent with the losses of D_2O and HOD respectively. The barrier for this process was not reported here, however, the barrier to the formation of the ion [Carnosine - H_2O - CO + H]$^+$ directly from [Carnosine + H]$^+$ was calculated to be 58.6 kcal mol^{-1} at B3LYP level.

[Histidine + H]$^+$, [Histidine – H_2O + H]$^+$ and [Histidine – H_2O – CO + H]$^+$

The last three ions observed at m/z values of 156, 138 and 110 as shown in Panel B of Figure 1 are assigned as [Histidine + H]$^+$, [Histidine – H_2O + H]$^+$ and as [Histidine – H_2O – CO + H]$^+$ respectively. The formation of [Histidine + H]$^+$ observed at m/z 156 through the loss of $CH(O)CH_2CHNH$ from [carnosine + H]$^+$ is consistent with the ion cluster around m/z 161 in the CID spectrum of the deuterium-incorporated complex shown in Figure S1 corresponding to the losses of two, one or none of the deuterium atoms from the precursor ion [carnosine-d_5 + D]$^+$ at ratios of 2:6:1. This is consistent with the pathway for the formation of this ion proposed here as shown in Figures 8 and 9 as well as Figure S4 in the supplementary material to initially involve two rearrangement steps of the precursor ion [carnosine + H]$^+$. The first of these rearrangement steps goes through the transition state $\mathbf{TS_{227\rightarrow227B}}$ and is calculated to require 57.7 kcal mol^{-1} when the B3LYP protocol is used, relative to structure **227**. This

barrier is, in fact, calculated to be significantly higher in energy than that needed for the eventual formation of the ion [Histidine + H]$^+$ observed at m/z 156 in Figure 1 Panel B as shown in structure **156** in Figures 8 and 9 from the rearranged form of the ion [Carnosine + H]$^+$ being structure **227C**. The corresponding transition state for this process being structure $\mathbf{TS_{227C\rightarrow 156}}$ is calculated at the B3LYP, M06, M06SP and MP2SP levels to be 36.0, 38.3, 37.9 and 36.6 kcal mol^{-1} relative to structure **227** respectively. In turn, the loss of H_2O from [Histidine + H]$^+$ to produce [Histidine – H_2O + H]$^+$ as observed at m/z 138 in Figure 1 Panel B and at m/z 141 and 142 in the CID spectrum of the deuterium-incorporated complex shown in Figure S1 corresponding to the retention of 3 and 4 deuterium atoms respectively is calculated to go through the transition state $\mathbf{TS_{156\rightarrow 138}}$ calculated at 64.9, 70.5, 81.6 and 72.8 kcal mol^{-1} respectively at the same levels of theory. Finally, the subsequent loss of CO from [Histidine – H_2O + H]$^+$ to produce the smallest observed ion [Histidine – H_2O – CO + H]$^+$ at m/z 110 in Figure 1 Panel B and at m/z 113 and 114 in the CID spectrum of the deuterium-incorporated complex shown in Figure S1 again corresponding to the retention of 3 and 4 deuterium atoms respectively is shown to involve a transition state at 62.1, 72.4, 80.4 and 72.7 kcal mol^{-1} for B3LYP, M06, M06SP and MP2SP respectively relative to structure **227** which is 19.3, 14.5, 23.1 and 17.9 kcal mol^{-1} lower than the barrier needed to produce its precursor. This may explain the observations presented in the collision induced dissociation curve of Figure 2 in which the ion [Histidine – H_2O + H]$^+$ at m/z 138 is shown not to attain any significant abundance while the ions [Histidine + H]$^+$ and [Histidine – H_2O – CO + H]$^+$ at m/z values of 156 and 110 respectively reach significant relative abundances.

The results of the computational analysis of the fragmentation pathways reported here shows that all the adopted computational protocols are able to reproduce and rationalize the experimental evidence and give comparable energetic trends. However, the description of the calculated energy profiles in terms of relative energies of the intercepted stationary points,

calculated with respect to the reference energy of structure **227**, appears to be significantly different when single point calculations are carried out on previously optimized geometries with the risk that the main features of the fragmentation PESs might not be captured.

Conclusions

Collision-induced dissociation experiments on protonated carnosine, $[Carnosine + H]^+$ using several collision energies were shown to yield eleven different fragment ions with the product ions $[Carnosine - H_2O + H]^+$ and $[Carnosine - NH_3 + H]^+$ to be the lowest energy processes. The MS^2 spectra of $[carnosine\text{-}d_5 + D]^+$ in which carnosine has all its labile hydrogen atoms exchanged with deuterium atoms provided some insights into the CID mechanisms although significant gas phase H/D scrambling prior to fragmentation was evident. The outcomes of the present combined theoretical and experimental investigation of the fragmentation pathways show that the lowest energy species for protonated carnosine found here is the same as that previously proposed [17, 21, 58]. The adopted computational protocols give comparable energetic trends and are all able to elucidate the fragmentation mechanisms, which account for all experimental data. However, when single point M06 and MP2 calculations on previously optimized B3LYP structures are carried out, the description of the energy profiles in some regions were significantly different.

Acknowledgements

The authors would like to thank the American University in Cairo for the funding sponsorship and provision of resources for the project. The Dipartimento di Chimica e Tecnologie Chimiche of Università della Calabria is also gratefully acknowledged.

References

[1] W. Gulewitsch, S. Amiradzibi, *Ber. Deut. Chem. Ges.* **1900**, *33*, 1902-1903.

[2] I. Severina, O. Bussygina, N. Pyatakova, *Biochemistry-Moscow* **2000**, *65*, 783-788.

[3] R. Kohen, Y. Yamamoto, K. Cundy, B. Ames, *Proc. Natl. Acad. Sci. U. S. A.* **1988**, *85*, 3175-3179.

[4] S.E. Gariballa, A. J. Sinclair, *Age and Aging* **2000***, 29***,** 207-210.

[5] M. Horning, L. Blakemore, P. Trombley, *Brain Res.* **2000**, *852*, 56-61.

[6] M. Nino, *Journal of cosmetics, dermatological sciences and applications* **2011***, 1*, 177.

[7] A.A. Boldyrev, *Biochemistry* (Moscow) **2000**, *65*, 751-756.

[8] A. Guiotto, A. Caderan, P. Ruzza, G. Borin *Curr. Med. Chem.* **2005**, *12*, 2293-2315.

[9] E.C. Smith, *J. Physiol.* **1938**, *92*, 336-343

[10] E.J. Baran, *Biochemistry* (Moscow) **2000**, *65*, 789-797.

[11] N.S. Nadi, J.D. Hirsch, F.L. Margolis, *J. Neurochem.* **1980**, *34*, 138-146.

[12] P. Hartman, Z. Hartman, K. Ault, *Photochemistry and photobiology* **1990***, 51*, 59-66.

[13] A. Pavlov, A. Revina, A. Dupin, A. Boldyrev, A. Yarpolov, *Biochimica et biophysica acta* **1993***, 1157*, 304-312.

[14] E.M. Moustafa, C.L. Camp, A.S. Youssef, A. Amleh, H.J. Reid, B.L. Sharp, T. Shoeib, *Metallomics* **2013**, *5*, 1537-1546.

[15] P. Mineo, *Rapid Commun. Mass Spectrom* **2002***, 16,* 722-729.

[16] M. Bjorn Reinhard, Chemistry of Microsolvated Metal Ions, Ph. D. Thesis, Kaiserslautern University of Technology, Germany, **2003**.

[17] F. Menges, C. Riehn, G. Niedner-Schatteburg, *Z. Phys. Chem.* **2011**, *225*, 595-609

[18] P.G. Peiretti, C. Medana, S. Visentin, V. Giancotti, V. Zunino, G. Meineri, *Food Chem.* **2011**, *126*, 1939-1947.

[19] S.A. Klyuev, *Biofizika* **2006**, *5*, 669-672.

[20] S.D. Demukhamedova, *J. Struct. Chem.* **2010**, *51*, 824-832.

[21] E.M. Moustafa, M. Korany, N. A. Mohamed, T. Shoeib, *Inorganica Chimica Acta* **2014**, *421*, 123-135.

[22] B. Paizs, S. Suhai, *Mass. Spectrom. Rev.* **2005**, ***24***, 508-548.

[23] N.N. Dookeran, T. Yalcin, A.G. Harrison, *J. Mass Spectrom.* **1996**, *31*, 500-508.

[24] T. Yalcin, A.G. Harrison, *J. Mass Spectrom.* **1996**, *31*, 1237-1243.

[25] F. Rogalewicz, Y. Hoppilliard, G. Ohanessian, *Int. J. Mass Spectrom.* **2000**, *195/196*, 565-590.

[26] H. El Aribi, G. Orlova, A.C. Hopkinson, K.W.M. Siu, *J. Phys. Chem. A*, **2004**, *108*, 3844-3853.

[27] R.A.J. O'Hair, M.L. Styles, G.E. Reid, *J. Am. Soc. Mass Spectrom.* **1998**, *9*, 1275-1284.

[28] H. Lioe, R.A.J. O'Hair, G.E. Reid, *J. Am. Soc. Mass Spectrom.* **2004**, *15*, 65-76.

[29] I.P. Csonka, B. Paizs, S. Suhai, *J. Mass Spectrom.* **2004**, *39*, 1025-1035.

[30] Z.B. Maksik, B. Kovacevic, *Chem. Phys. Lett.* **1999**, *307*, 497–504.

[31] A.K.Y. Lam, S.H. Ramarathinam, A.W. Purcell, R.A.J. O'Hair, *J. Am. Soc. Mass. Spectrom.* **2008**, *19*, 1743-1754.

[32] E.R. Talaty, T.J. Cooper, S. Osburn ,M.J. Van Stipdonk, *Rapid Commun. Mass. Spectrom.* **2006**, *20*, 3443–3455.

[33] T. Shoeib, A. Cunje, A.C. Hopkinson, K.W.M. Siu, *J. Am. Soc. Mass Spectrom.* **2002**, *13*, 408-416.

[34] H. Lioe, R.A.J. O'Hair, *Org. Biomol. Chem.* **2005**, *3*, 3618-3628.

[35] E. Uggerud, *Theor. Chim. Acta* **1997**, *97*, 313-316.

[36] F. Rogalewicz, Y. Hoppilliard, G. Ohanessian, *Int. J. Mass Spectrom.* **2000**, *195/196*, 565-590.

[37] I. Ritacco, E. M. Moustafa, E. Scicilia, N. Russo, T. Shoeib, *Dalton Trans.*, **2015**, *44*, 4455-4467.

[38] S. L. Kerr, T. Shoeib, B. L. Sharp, *Anal. Bioanal. Chem.* **2008**, *391*, 2339-2348.

[39] T. Shoeib, D. W. Atkinson and B. L. Sharp, *Inorg. Chim. Acta.* **2010**, *363*, 184-192.

[40] T. Shoeib, I.K. Chu, Y.-P. Tu, A.C. Hopkinson and K.W.M. Siu, *Eur. J. Mass Spectrom.* **2000**, 6, *187*-192.

[41] C.F. Rodriquez, X. Guo, T. Shoeib, A.C. Hopkinson and K.W.M. Siu, *J. Am. Soc. Mass Spectrom.* **2000**, *11*, 967-975.

[42] T. Shoeib, J. Zhao, H. El Aribi, A. C. Hopkinson, K.W.M. Siu, *J. Am. Soc. Mass Spectrom.* **2013**, *24*, 38-48.

[43] M.J. Frisch, G.W. Trucks, H.B. Schlegel, G.E. Scuseria, M.A. Robb, J.R. Cheeseman, G. Scalmani, V. Barone, B. Mennucci, G.A. Petersson, H. Nakatsuji, M. Caricato, X. Li, H.P. Hratchian, A.F. Izmaylov, J. Bloino, G. Zheng, J.L. Sonnenberg, M. Hada, M. Ehara, K. Toyota, R. Fukuda, J. Hasegawa, M. Ishida, T. Nakajima, Y. Honda, O. Kitao, H. Nakai, T. Vreven, J.A. Montgomery Jr., J.E. Peralta, F. Ogliaro, M. Bearpark, J.J. Heyd, E. Brothers, K.N. Kudin, V.N. Staroverov, R. Kobayashi, J. Normand, K. Raghavachari, A. Rendell, J.C. Burant, S.S. Iyengar, J. Tomasi, M.

Cossi, N. Rega, J.M. Millam, M. Klene, J.E. Knox, J.B. Cross, V. Bakken, C. Adamo, J. Jaramillo, R. Gomperts, R.E. Stratmann, O. Yazyev, A.J. Austin, R. Cammi, C. Pomelli, J.W. Ochterski, R.L. Martin, K. Morokuma, V.G. Zakrzewski, G.A. Voth, P. Salvador, J.J. Dannenberg, S. Dapprich, A.D. Daniels, O¨. Farkas, J.B. Foresman, J.V. Ortiz, J. Cioslowski, D.J. Fox, Gaussian 09, Revision A.1, Gaussian Inc, Wallingford CT, **2009**.

[44] A. Lee, W. Yang, R. G. Parr, *Phys. Rev. B* **1988**, *37*, 785-789.

[45] A. D. Becke, *Phys. Rev. A* **1988**, *38*, 3098-3100.

[46] A. D. Becke, *J. Chem. Phys.* **1993**, *98*, 5648–5652.

[47] R. Krishnan, J.S. Binkley, R. Seeger, J.A. Pople, *J. Chem. Phys.* **1980**, *72*, 650-654.

[48] J.P. Blaudeau, M.P. McGrath, L.A. Curtiss, L. Radom, *J. Chem. Phys.* **1997**, *107*, 5016-5021.

[49] T. Clark, J. Chandrasekhar, P. V. R. Schleyer, *J. Comp. Chem.* **1983**, *4*, 294-301.

[50] K. Fukui, *Acc. Chem. Res.* **1981**, *14*, 363-68.

[51] R. C. Guedes, P. C. Do Couto, B. J. C. Cabral, *J. chem. Phys.* **2003**, *118*, 1272-1281.

[52] R. K. Milburn, A. C. Hopkinson, D. K. Bohme, *J. Am. Chem. Soc.* **2005**, *127*, 13070-13078

[53] X. Xu, W. A. Goddard, *J. Phys. Chem. A* **2004**, *108*, 2305-2313.

[54] K. Schoone, J. Smets, R. Ramaekers, L. Houben, L. Adamowicz, G. Maes, *J. Mol. Struct.* **2003**, *649*, 61-68.

[55] H. El Aribi, C. F. Rodriquez, D. R. P. Almeida, Y. Ling, W. W. N. Mak, A. C. Hopkinson, K. W. M. Siu, *J. Am. Chem. Soc.* **2003**, *125*, 9229-9236.

[56] C. Moller, M.S. Plesset, *Phys. Rev.* **1934**, *46*, 618-622.

[57] Y. Zhao, D.G. Truhlar, *Theor. Chem.. Account* **2008**, *120*, 215-241.

[58] G. Grégoire, M.P. Gaigeot, D.C. Marinica, J. Lemaire, J.P. Schermann, C. Desfrançois, *Phys. Chem. Chem. Phys.*, **2007**, *9*, 3082-3097.

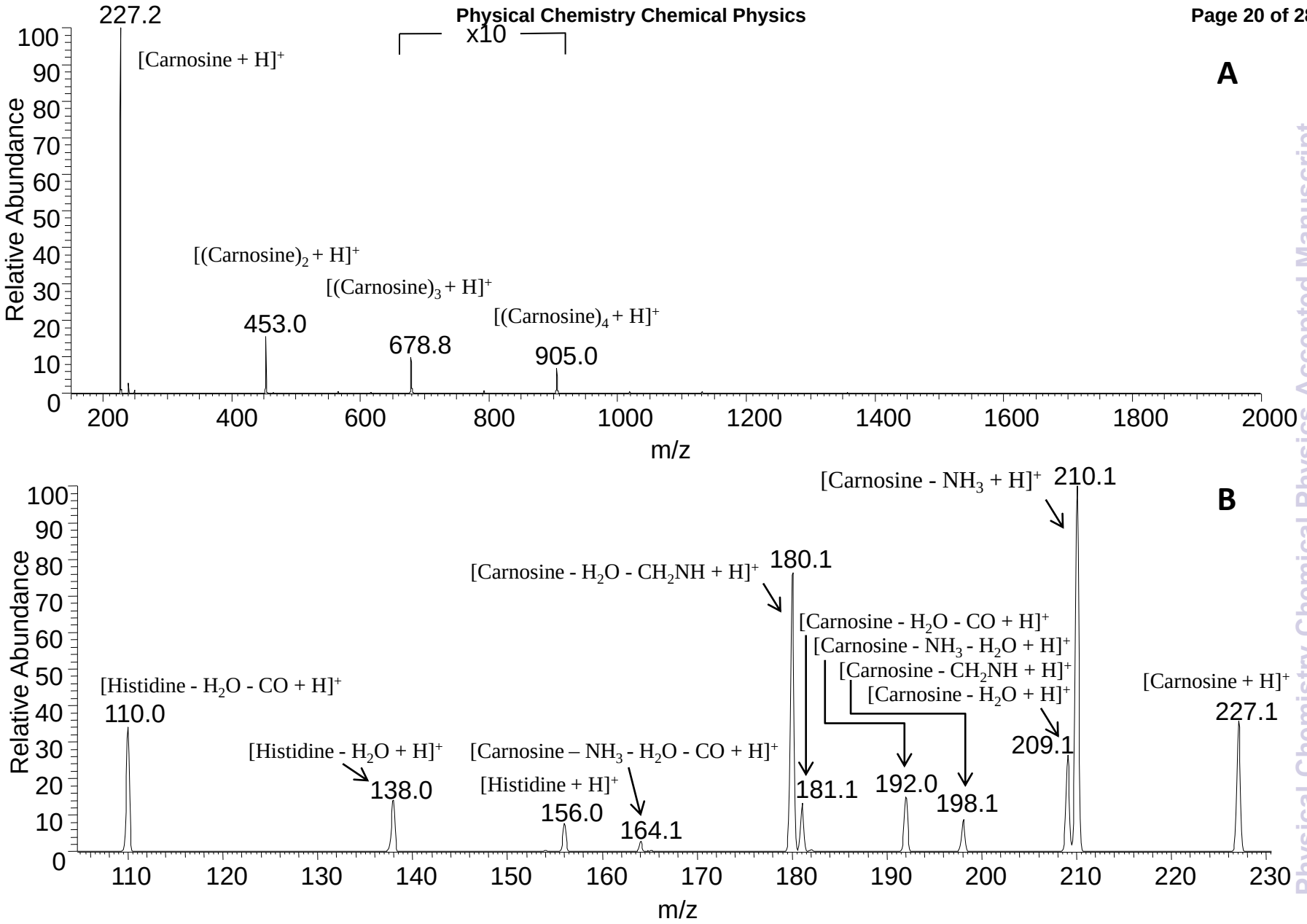

Figure 1: Panel A, full scan MS spectrum of a 1mM of Carnosine in a (1:1) (v/v) water/methanol solution as without allowing for incubation time. Panel B, MS^2 spectrum of the ion $[Carnosine + H]^+$ generated at 25 eV in the lab frame. Both mass spectra were generated by an LTQ linear ion trap using helium as a collision gas as described in the instrumental section.

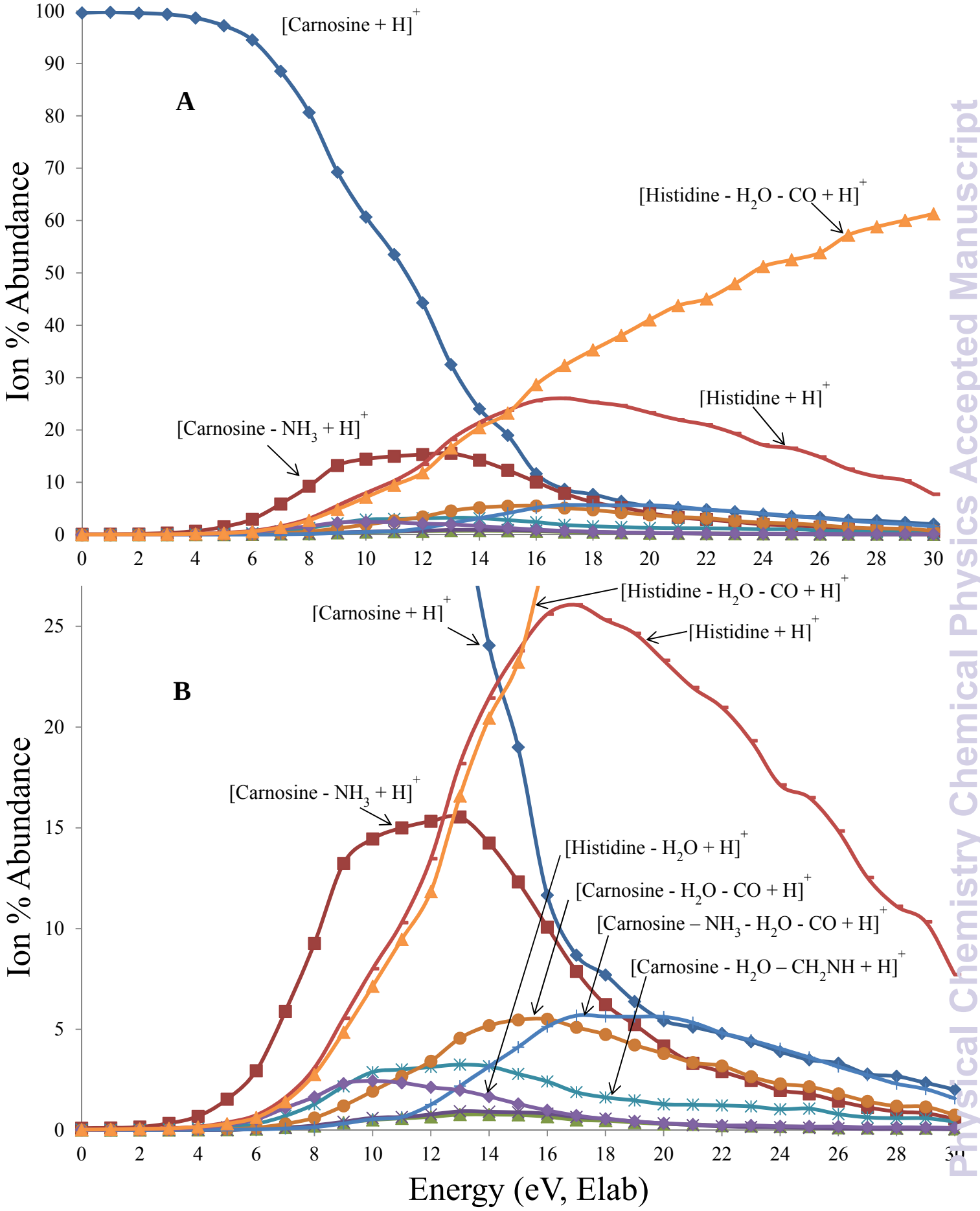

Figure 2: Energy-resolved collision induced dissociation curves of $[Carnosine + H]^+$ as obtained on the Aquity TQ tandem mass spectrometer employing argon as a collision gas as described in the instrumental section. Y-axis are (ion abundance)/(total ion abundance) expressed as a percentage. Panel A shows the full curve while panel B shows an expanded view for clarity. Only ions attaining relative intensities above 2.5% are labelled.

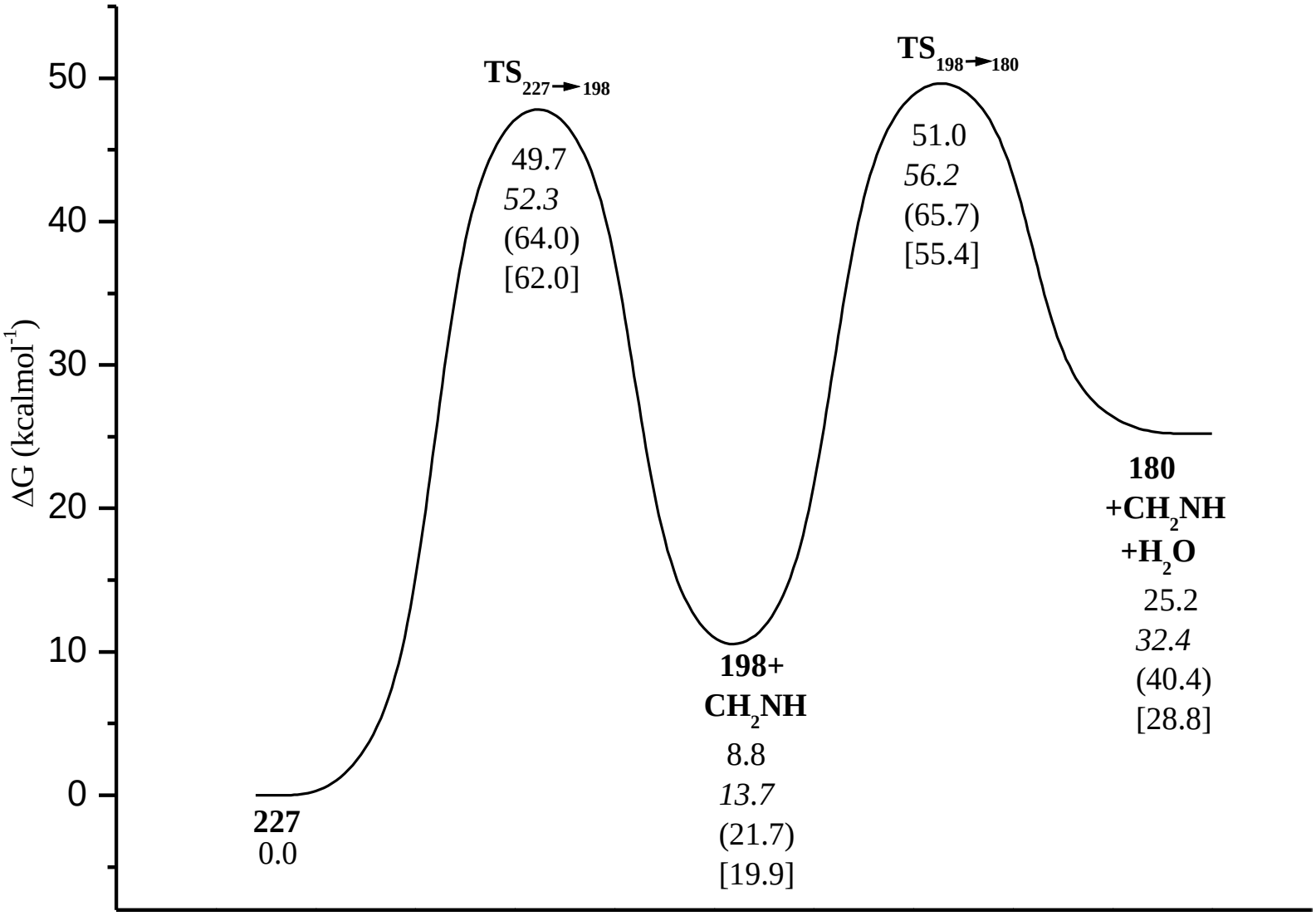

Figure 3: B3LYP free energy profile for the fragmentation of [Carnosine + H]$^+$ to give the ion at m/z 180 and its precursor at m/z 198. Relative free energies at 298 K are in kcal mol^{-1} and calculated with respect to the most stable conformer, **227,** of protonated carnosine. M06, M06SP and MP2SP values are reported in italics, in brackets and square brackets, respectively.

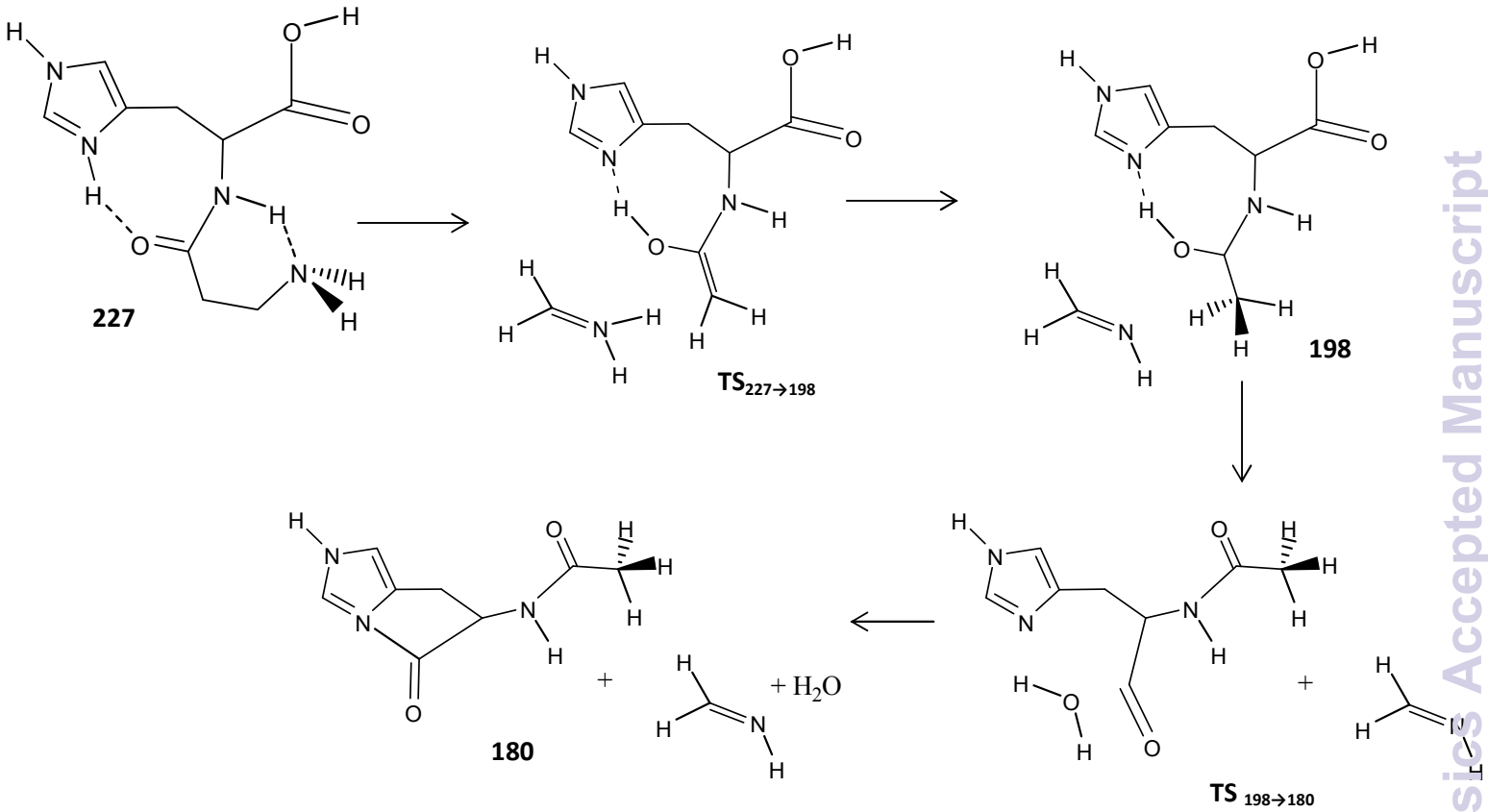

Figure 4: Proposed mechanism for the collision induced fragmentation of [Carnosine + H]$^+$ to produce the fragments observed at m/z 198 and 180.

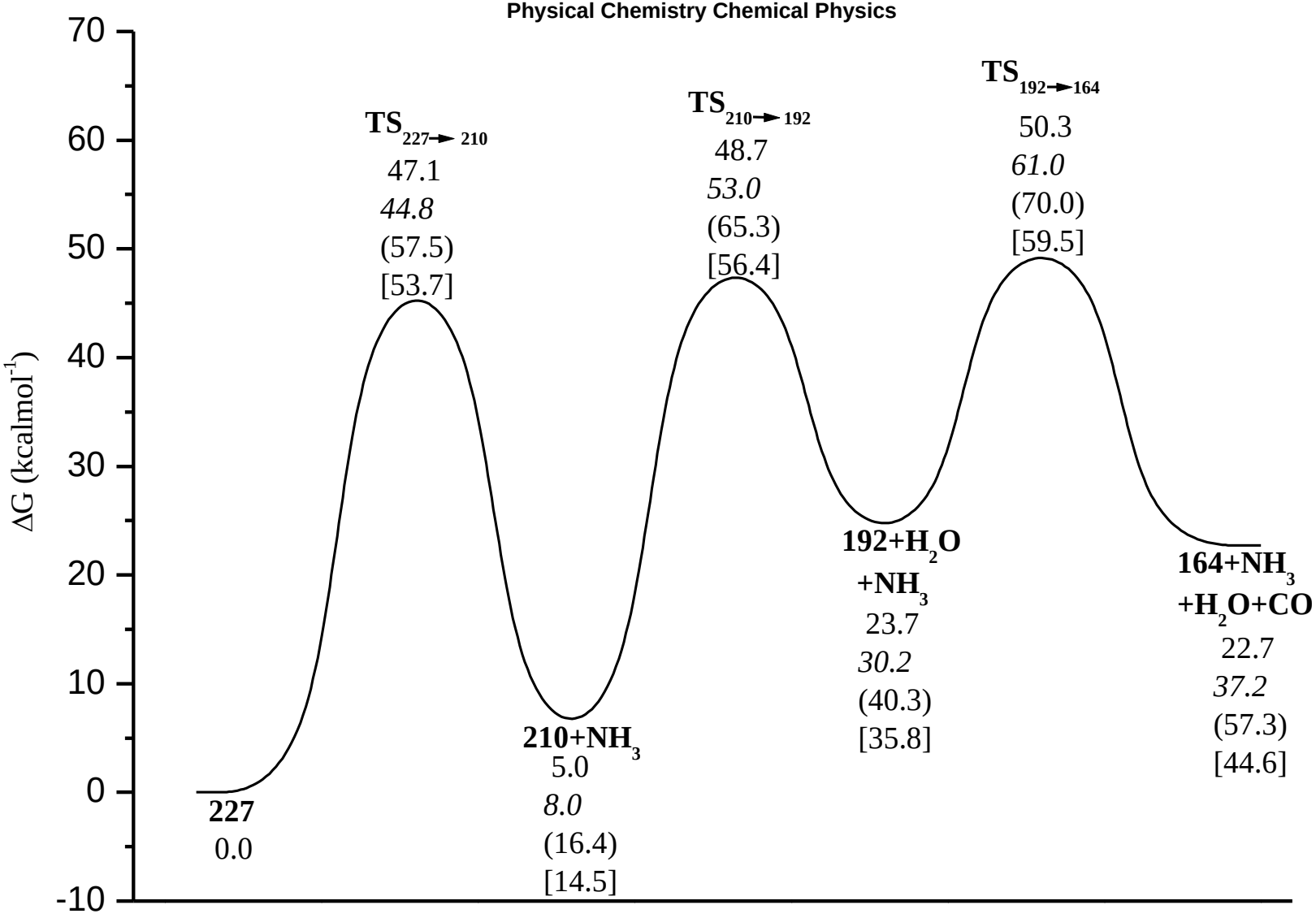

Figure 5: B3LYP free energy profile for the fragmentation of [Carnosine + H]$^+$ to give the ion at m/z 164 and its precursors at m/z 210 and 192. Relative free energies at 298 K are in kcal mol^{-1} and calculated with respect to the most stable conformer, **227,** of protonated carnosine. M06, M06SP and MP2SP values are reported in italics, in brackets and square brackets, respectively.

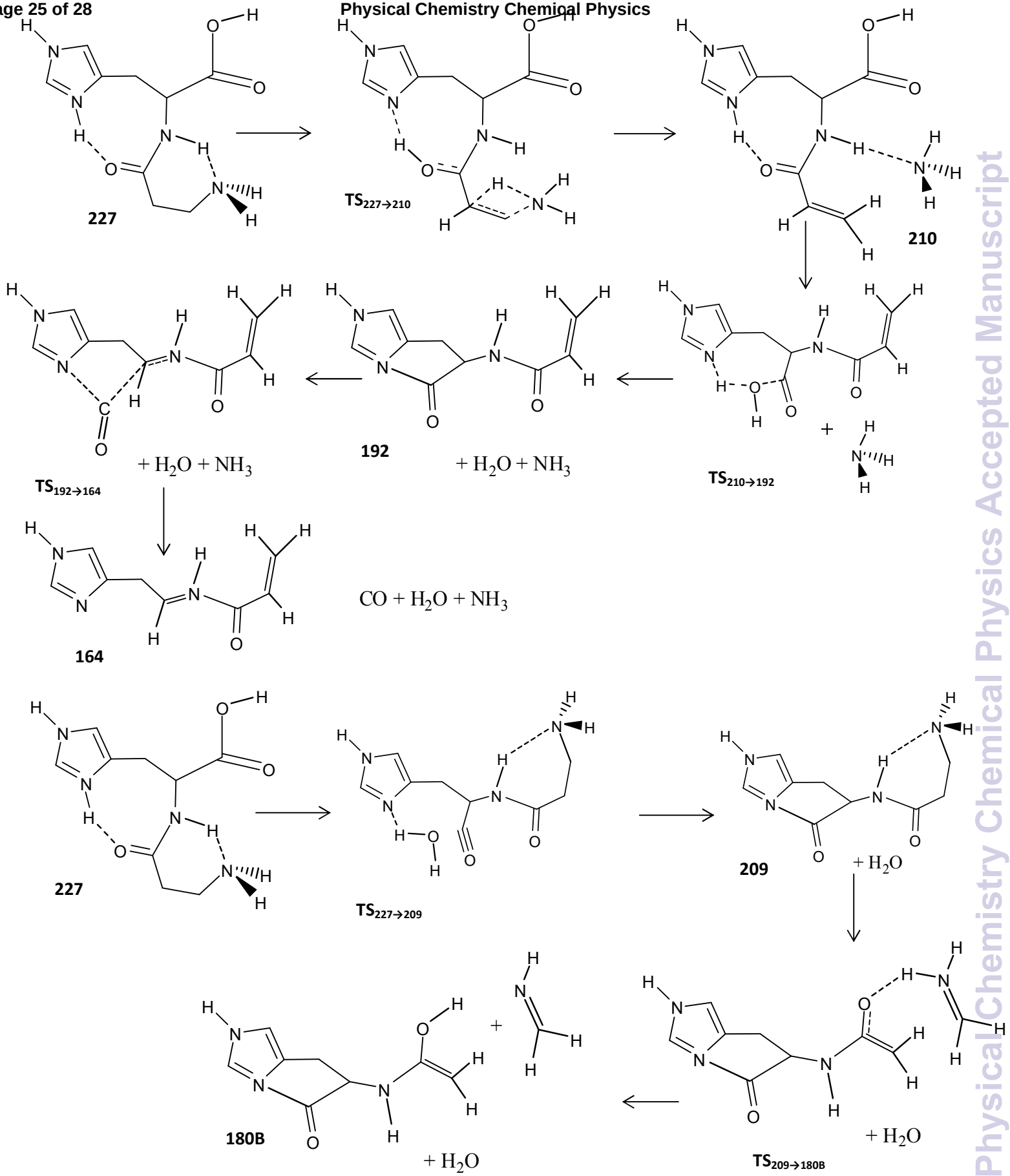

Figure 6: Proposed mechanism for the collision induced fragmentation of [Carnosine + H]$^+$ to produce the fragments observed at m/z 210, 192 and 164.

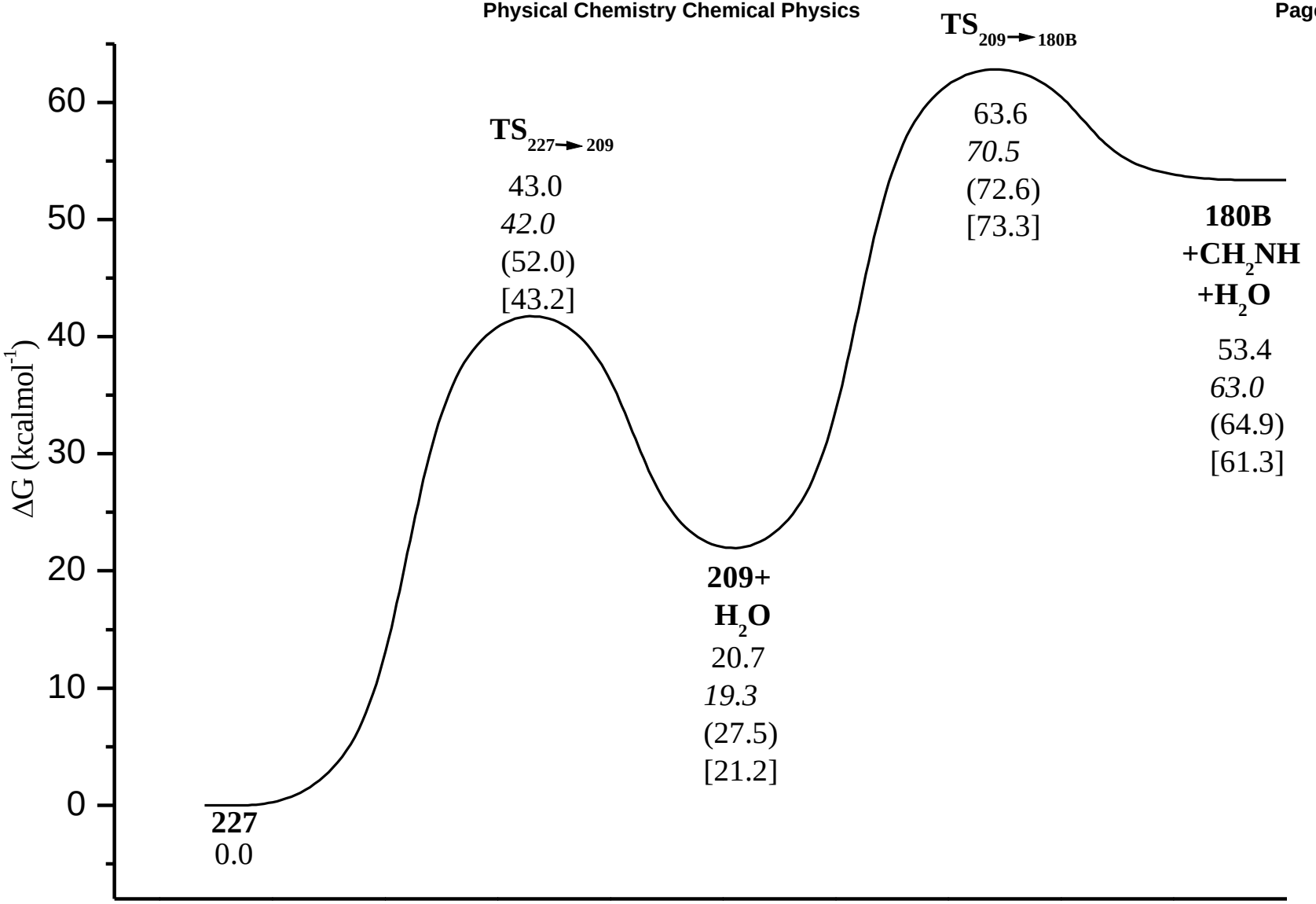

Figure 7. B3LYP free energy profile for the fragmentation of [Carnosine + H]$^+$ to give the ion at m/z 180 and its precursor at m/z 209. Relative free energies at 298 K are in kcal mol^{-1} and calculated with respect to the most stable conformer, **227,** of protonated carnosine. M06, M06SP and MP2SP values are reported in italics, in brackets and square brackets, respectively.

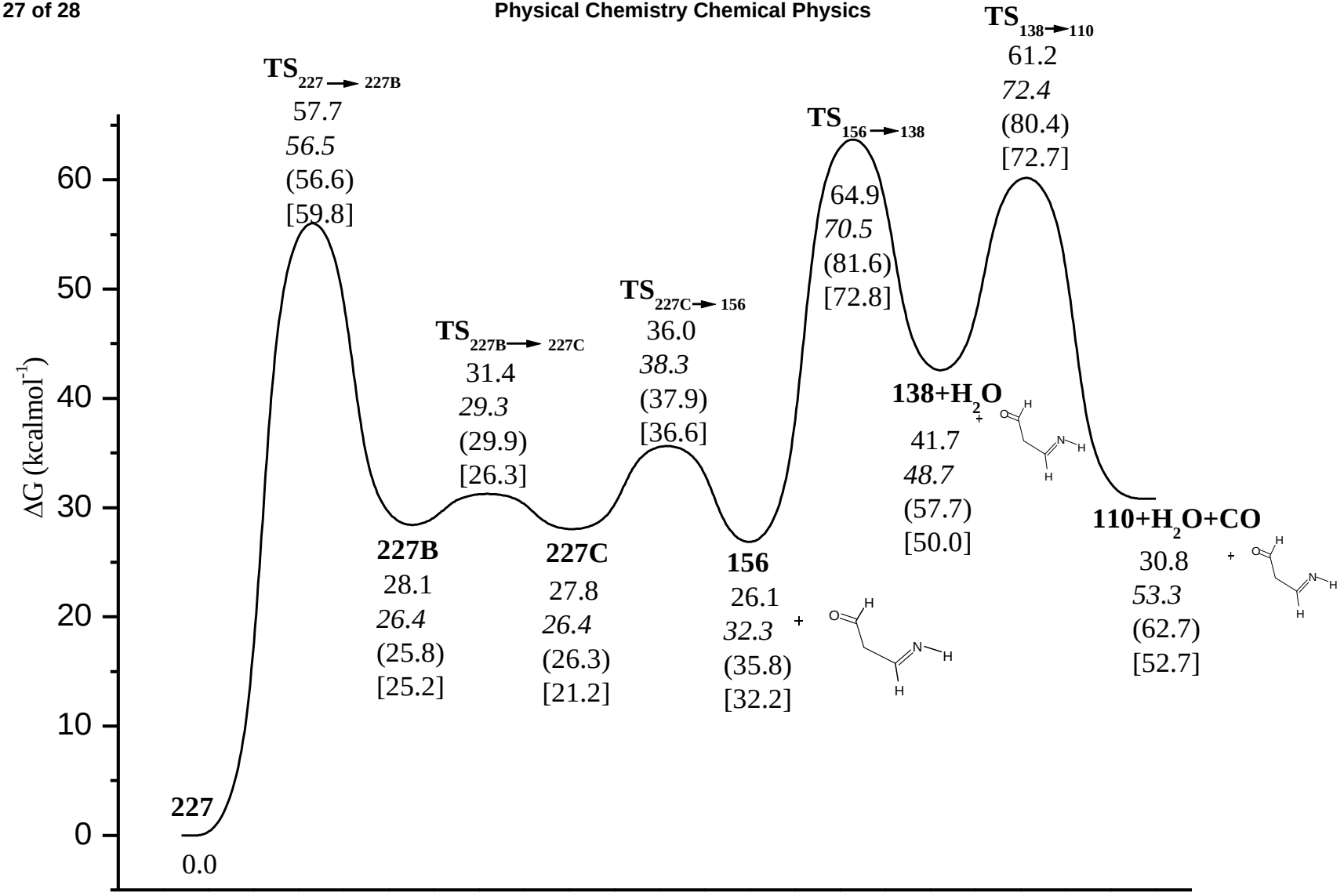

Figure 8: B3LYP free energy profile for the fragmentation of [Carnosine + H]$^+$ to give the ion at m/z 110 and its precursors at m/z 138, 156 and 227. Relative free energies at 298 K are in kcal mol^{-1} and calculated with respect to the most stable conformer, **227,** of protonated carnosine. M06, M06SP and MP2SP values are reported in italics, in brackets and square brackets, respectively.

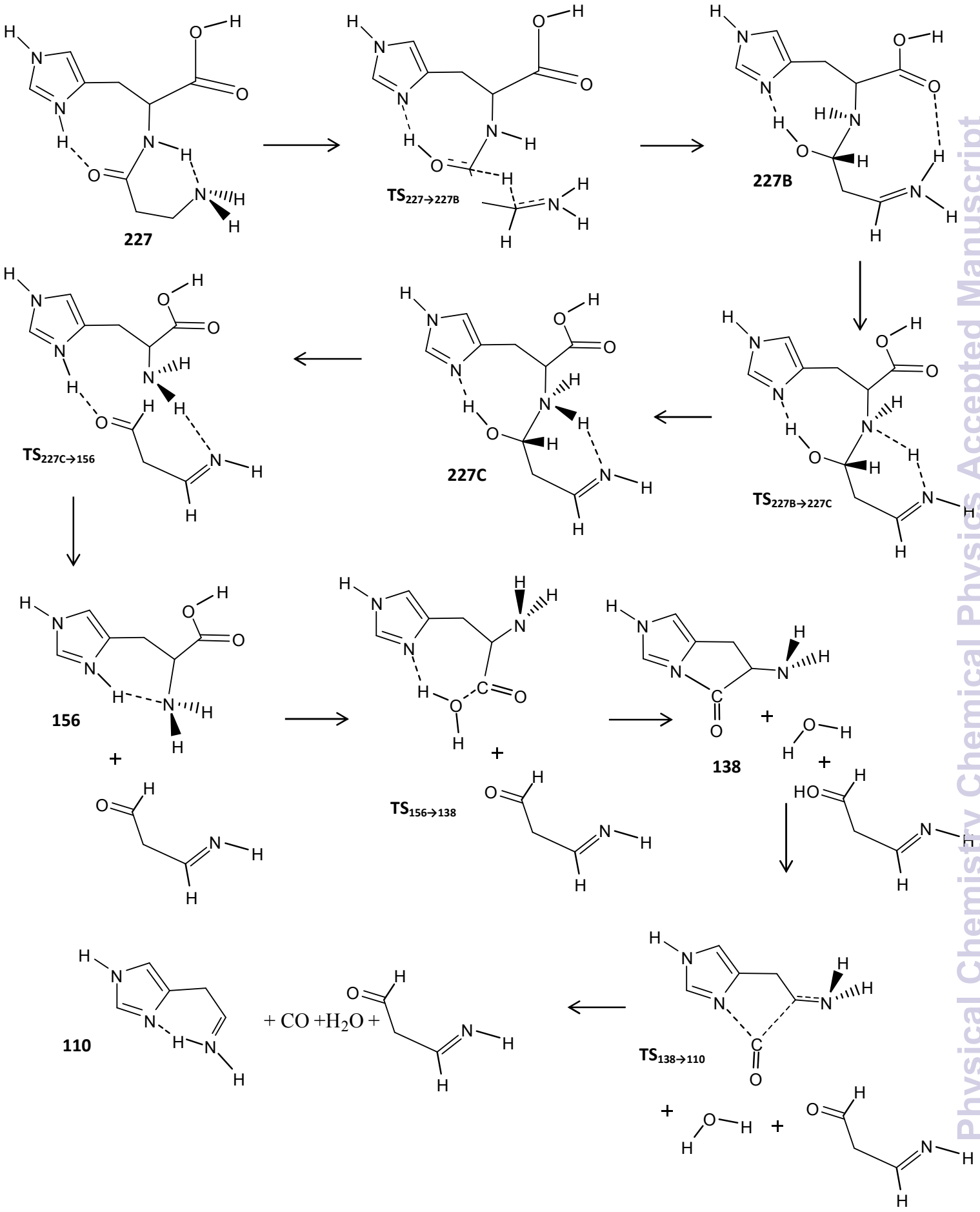

Figure 9: Proposed mechanism for the collision induced fragmentation of [Carnosine + H]$^+$ to produce the fragment ion observed at m/z 156, 138 and 110.